Model Predictive Control of Grid-Connected Inverters for PV Systems With Flexible Power Regulation and Switching Frequency Reduction

Jiefeng Hu, *Member, IEEE*, Jianguo Zhu, *Senior Member, IEEE*, and David G. Dorrell, *Senior Member, IEEE*

***Abstract*—This paper presents a model predictive direct power control strategy for a grid-connected inverter used in a photovoltaic system as found in many distributed generating installations. The controller uses a system model to predict the system behavior at each sampling instant. The voltage vector that generates the least power ripple is selected using a cost function and applied during the next sampling period; thus, flexible power regulation can be achieved. In addition, the influence of a one-step delay in the digital implementation is investigated and compensated for using a model-based prediction scheme. Furthermore, a two-step horizon prediction algorithm is developed to reduce the switching frequency, which is a significant advantage in higher power applications. The effectiveness of the proposed model predictive control strategy was verified numerically by using MATLAB/Simulink and validated experimentally using a laboratory prototype.**

***Index Terms*—Inverters, model predictive control (MPC), power regulation, switching frequency reduction.**

I. Introduction

BECAUSE OF the drive to move away from fossil fuel and various government policies aimed at reducing carbon dioxide emissions, distributed generation (DG) units are increasingly being deployed and connected to the local low-voltage power system through a power converter. Photovoltaic (PV) panels are the most common form of DG, while there may also be fuel cell systems and smaller wind turbines [1]–[3]. In order to obtain more capacity and control flexibility, which leads to improved system reliability and power quality, these DGs are integrated into a common ac or dc bus with an energy storage system to form a microgrid [4], [5].

Another promising characteristic of a DG system is its grid support capacity. The stabilization of the power system is a challenging task due to fluctuating load demands. In this sense, DGs should be used and controlled to provide active power and reactive power compensation to help stabilize the main power system in terms of voltage and frequency [6]. Therefore, a DG power converter is required to operate more efficiently and effectively to maintain high power quality and dynamic stability.

There are various existing control strategies for grid-connected inverters, among which direct power control (DPC) is one of the most popular control approaches. Conventional switching-table-based DPC (SDPC) has been widely used because of its advantages such as simplicity, robustness, and excellent transient response [7]. Later, many improved DPC methods had been developed to achieve better performances [8]–[10].

Model predictive control (MPC) appears to be an attractive alternative for the control of a power converter because it has a flexible control scheme that allows the easy inclusion of system constraints and nonlinearities. In this control, a system model is used to predict the system behavior using the present states and the control action. A cost function is then employed as a criterion to select the optimal switching states. The control objectives of MPC can vary considerably according to the application. For example, the control objectives are active and reactive powers for rectifiers [11]–[13], electromagnetic torque for electric drives [14], [15], and the voltage or current for inverter systems [16]–[19]. However, so far, very little has been reported on flexible power regulation for a grid-connected inverter using MPC strategies. Flexible power regulation is very essential for DGs because frequency regulation by active power control and voltage support by reactive power compensation is required after grid connection. More recently, a model predictive DPC (MPDPC) for a grid-connected inverter with an LCL filter was developed in [20]. The power injected into the grid was not controlled directly due to the filter capacitance. In addition, the additional poles introduced by the LC part induce resonance into the system, leading to stability issues.

There is a perception that there is a clear tendency to increase the power capacity and voltage level with the purpose of increasing the efficiency in distributed-power generation. However, relatively high switching frequency will cause a large power loss [21]. Consequently, attention has been paid to switching frequency reduction in the control of a power converter [18], [19].

By taking the advantage of the flexibility of the MPC approach, this paper proposes an MPDPC strategy for a grid-connected inverter in a PV system. A cost function is first defined to reduce the active and reactive power ripples. Next,

Manuscript received November 14, 2013; revised March 18, 2014; accepted May 27, 2014. Date of publication June 4, 2014; date of current version January 16, 2015. Paper 2013-SECSC-872.R1, presented at the 2013 IEEE Energy Conversion Congress and Exposition, Denver, CO, USA, September 16–20, and approved for publication in the IEEE TRANSACTIONS ON INDUSTRY APPLICATIONS by the Sustainable Energy Conversion Systems Committee of the IEEE Industry Applications Society.

J. Hu is with the School of Automation Science and Electrical Engineering, Beihang University, Beijing 100191, China (e-mail: jhu@buaa.edu.cn).

J. Zhu and D. G. Dorrell are with the Faculty of Engineering and Information Technology, University of Technology Sydney, Sydney, N.S.W. 2007, Australia (e-mail: Jianguo.Zhu@uts.edu.au; David.Dorrell@uts.edu.au).

Color versions of one or more of the figures in this paper are available online at http://ieeexplore.ieee.org.

Digital Object Identifier 10.1109/TIA.2014.2328785

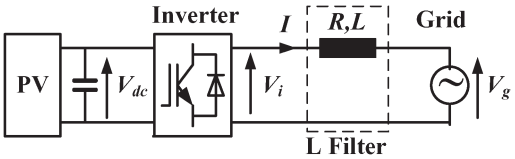

Fig. 1. One-phase model of the grid-connected PV system.

a model-based prediction scheme is developed to compensate for a one-step delay in the digital implementation. In order to reduce the inverter switching loss, a two-step horizon prediction algorithm $(N = 2)$ is developed. Both simulation and experimental results validate the effectiveness of the proposed control strategy.

II. System Modeling

Fig. 1 shows a PV system connected to the grid through an inverter. Generally, a PV system consists of a dc–dc converter and an inverter. The maximum power tracking is implemented in the dc–dc converter while the inverter is used to convert the dc voltage to ac voltage [22]. In this paper, the grid-side inverter is focused upon. The voltage of a three-phase two-level inverter is determined by the switching states and can be controlled to seven vectors

$$V_i = \begin{cases} \frac{2}{3}V_{\rm dc}e^{j(i-1)\frac{\pi}{3}}, & i = 1, \ldots, 6 \\ 0, & i = 0, 7. \end{cases} \tag{1}$$

Transforming the voltage vectors from the three-phase abc-frame to the orthogonal $\alpha\beta$-frame yields the $\alpha\beta$ components: $V_i = [V_{i\alpha}\ V_{i\beta}]^{\rm T}$. Subsequently, the mathematical model of the grid-connected inverter system can be described in orthogonal $\alpha\beta$-frame

$$V_i = L\frac{dI}{dt} + RI + V_g \tag{2}$$

where $V_g = [V_{g\alpha}\ V_{g\beta}]^{\rm T}$ is the grid voltage and $I = [I_\alpha\ I_\beta]^{\rm T}$ is the line current. Considering sinusoidal and balanced grid voltage, one can obtain

$$\frac{dV_{g\alpha}}{dt} = -\omega \cdot V_{g\beta} \tag{3}$$

$$\frac{dV_{g\beta}}{dt} = \omega \cdot V_{g\alpha} \tag{4}$$

where ω is the frequency of grid voltage in radians per second. Equations (2)–(4) can be rewritten as a state-space system

$$\frac{dx}{dt} = Ax + BV_i \tag{5}$$

where

$$x = [\, I_\alpha \quad I_\beta \quad V_{g\alpha} \quad V_{g\beta}\,]^{\rm T} \tag{6}$$

$$A = \begin{bmatrix} -\frac{R}{L} & 0 & -\frac{1}{L} & 0 \\ 0 & -\frac{R}{L} & 0 & -\frac{1}{L} \\ 0 & 0 & 0 & -\omega \\ 0 & 0 & \omega & 0 \end{bmatrix} \tag{7}$$

$$B = \begin{bmatrix} \frac{1}{L} & 0 \\ 0 & \frac{1}{L} \\ 0 & 0 \\ 0 & 0 \end{bmatrix}. \tag{8}$$

In this state-space system, I and V_g are the state variables and are measured, while V_i is the input.

III. Proposed MPDPC Controller

The aim of the MPDPC controller is to enable flexible power regulation and switching frequency reduction.

A. Flexible Power Regulation

In order to achieve flexible power regulation, the system model uses active and reactive powers as the state variables. These should be obtained for the design of the MPDPC controller. However, the system model in (5) uses the line current and grid voltage as the state variables, and it is not related directly to the output power. Consequently, an accurate model for active and reactive powers is required, which is one of the challenging tasks of this work.

The instantaneous active and reactive powers injected into the grid by the grid-connected inverter system can be described as a state equation, where

$$y = \begin{bmatrix} P \\ Q \end{bmatrix} = \frac{3}{2}\begin{bmatrix} V_{g\alpha} & V_{g\beta} \\ V_{g\beta} & -V_{g\alpha} \end{bmatrix}\begin{bmatrix} I_\alpha \\ I_\beta \end{bmatrix}. \tag{9}$$

The active and reactive power derivatives with respect to time t can be derived from (9) as

$$\begin{bmatrix} \frac{dP}{dt} \\ \frac{dQ}{dt} \end{bmatrix} = \frac{3}{2}\begin{bmatrix} \frac{dV_{g\alpha}}{dt} & \frac{dV_{g\beta}}{dt} \\ \frac{dV_{g\beta}}{dt} & -\frac{dV_{g\alpha}}{dt} \end{bmatrix}\begin{bmatrix} I_\alpha \\ I_\beta \end{bmatrix} + \frac{3}{2}\begin{bmatrix} V_{g\alpha} & V_{g\beta} \\ V_{g\beta} & -V_{g\alpha} \end{bmatrix}\begin{bmatrix} \frac{dI_\alpha}{dt} \\ \frac{dI_\beta}{dt} \end{bmatrix}. \tag{10}$$

Combining (5), (9), and (10) yields

$$\frac{dy}{dt} = Cy + \frac{3}{2L}DV_i - \frac{3}{2L}EV_g \tag{11}$$

where

$$C = \begin{bmatrix} -\frac{R}{L} & -\omega \\ \omega & -\frac{R}{L} \end{bmatrix} \tag{12}$$

$$D = \begin{bmatrix} V_{g\alpha} & V_{g\beta} \\ V_{g\beta} & -V_{g\alpha} \end{bmatrix} \tag{13}$$

$$E = \begin{bmatrix} V_{g\alpha} & V_{g\beta} \\ 0 & 0 \end{bmatrix}. \tag{14}$$

It can be seen that the grid-connected inverter system is now represented by a state-space system with P and Q as the state variables and V_i as the input; V_g can be measured. A discrete-time model of (11) for a sampling time T_s is

$$y(k+1) = y(k) + \left[Cy(k) + \frac{3}{2L}DV_i(k) - \frac{3}{2L}EV_g(k)\right]T_s. \tag{15}$$

Since the sampling time T_s is very small, it can be assumed that

$$e^{CT_s} = 1 + CT_s + \frac{(CT_s)^2}{2!} + \cdots + \frac{(CT_s)^n}{n!} \approx 1 + CT_s. \tag{16}$$

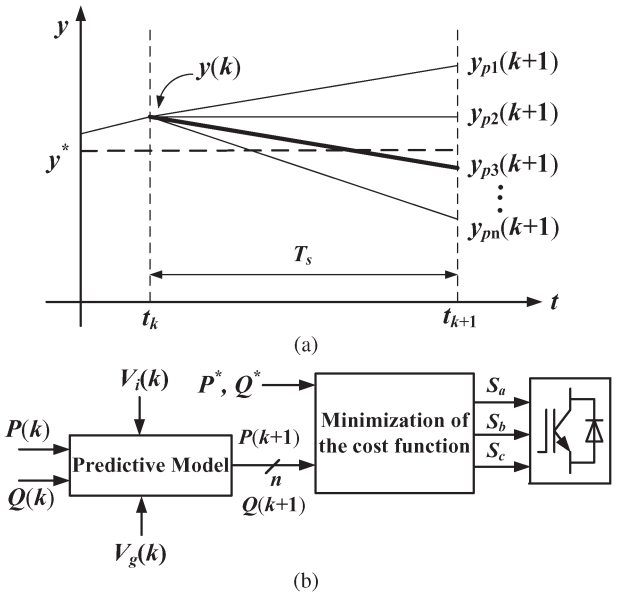

Fig. 2. Illustration of MPDPC controller. (a) Voltage vector evaluation and selection. (b) Block diagram.

Therefore, the discrete-time model of (15) can be further simplified to

$$y(k+1) = C_d y(k) + \frac{3}{2L} D_d V_i(k) - \frac{3}{2L} E_d V_g(k) \qquad (17)$$

where

$$C_d = e^{CT_s} \qquad (18)$$

$$D_d = \int_0^{T_s} e^{C\tau} D \, d\tau \qquad (19)$$

$$E_d = \int_0^{T_s} e^{C\tau} E \, d\tau. \qquad (20)$$

This equation can be used as the predictive model in the proposed MPDPC controller. Fig. 2(a) clearly illustrates the essential properties of the MPDPC strategy. All possible system transitions $y_{pi}(k+1)$ can be predicted using the discrete-time model of the system for all control actions (or the time horizon) of $N\,(N = 1, 2, 3, \ldots, n)$. Take $N = 1$ as an example; the system behavior at $k+1$ instant can be predicted with the measured value $y(k)$ and n possible voltage vectors, resulting in n possible values $y_{p1}, y_{p1}, \ldots, y_{pn}$. Now, suppose that y_{p3} is closest to y^*; the voltage vector producing y_{p3} will be selected and applied between the k and $(k+1)$ instants.

Fig. 2(b) depicts the MPDPC control strategy for a grid-connected inverter system in order to obtain flexible power regulation. The measurements of the line currents and grid voltages are used to calculate the active power $P(k)$ and reactive power $Q(k)$. The values at the next sampling instant $P(k+1)$ and $Q(k+1)$, for all possible voltage vectors, can be predicted using the discrete-time model (17). To select the optimal voltage vector, all predicted powers are compared

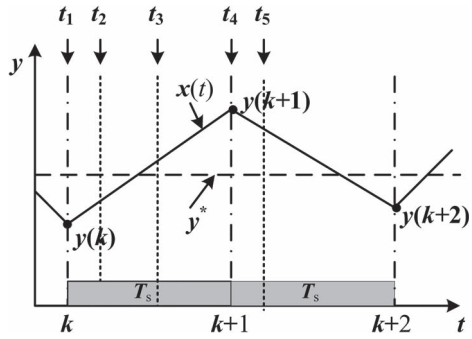

Fig. 3. Data processing in a DSP.

using a cost function, and the voltage vector that minimizes this cost function is chosen and applied at the next sampling period. Here, since the active and reactive powers have the same priority for flexible power regulation, the following cost function is utilized. To minimize the power error

$$J = (P^* - P(k+1))^2 + (Q^* - Q(k+1))^2 \qquad (21)$$

where P^* is the reference active power and Q^* is the reactive power. This cost function has been chosen in order to minimize the power errors so that the grid-connected inverter system can inject any amount of active and reactive powers within its capacity. This is a very useful attribute for DG units.

B. One-Step Delay Compensation in Digital Implementation

Fig. 3 illustrates the process of the control algorithm execution in the digital hardware system. The system controlled variable $y(k)$ is sampled at $t = t_1$, and the analog-to-digital conversion process is completed at $t = t_2$. The calculation of the appropriate voltage vector is finished at $t = t_3$, but it is not applied until the next sampling instant at $t = t_4$. This is the one-step delay. Now, an in-depth analysis of the one-step delay is performed. After the desired voltage vector $\boldsymbol{V}_i(k)$ is determined using $y(k)$ and y^* at $t = t_3$, it will not be applied until the $(k+1)$th instant. However, the variables at the $(k+1)$th instant have evolved into $y(k+1)$, which will usually be different from $y(k)$ due to the application of $\boldsymbol{V}_i(k-1)$. As a result, the vector applied at the $(k+1)$th instant, which is determined based on $y(k)$, may no longer be the best one. Therefore, $y(k+1)$ should be employed to determine the desired voltage $V_i(k)$, which will reduce the error at the $(k+2)$th instant with respect to the reference value y^*.

In this paper, a new two-step prediction scheme is developed in order to incorporate a one-step delay compensation with MPC strategy. $P(k+1)$ and $Q(k+1)$ are first obtained from (17). Assuming that the grid voltage is constant during the sampling period, $P(k+2)$ and $Q(k+2)$ can then be predicted using $P(k+1)$ and $Q(k+1)$ as the new initial state variables and $\boldsymbol{V}_i(k)$ as the input. Consequently, the cost function in (21) should be revised to

$$J = (P^* - P(k+2))^2 + (Q^* - Q(k+2))^2 . \qquad (22)$$

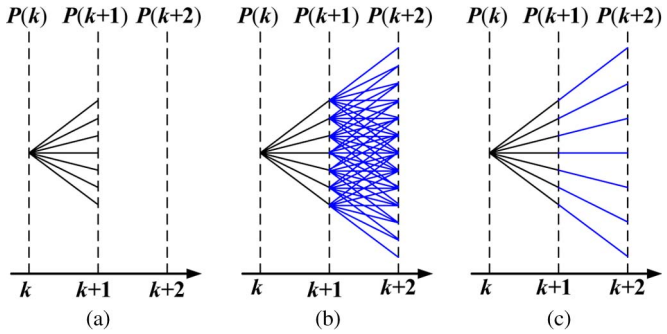

Fig. 4. Illustration of prediction scheme. (a) $N = 1$. (b) $N = 2$ considering different vectors during each sampling period. (c) $N = 2$ considering the same vectors during two sampling periods.

C. Switching Frequency Reduction

In distributed-power generation, the lower the switching frequency is, the less the power loss will be produced, i.e., higher efficiency can be obtained. In order to reduce the switching frequency, a two-step prediction horizon is employed. When only one-step prediction is considered, eight voltage vectors are evaluated during one sampling period. For a prediction horizon of $N = 2$, one voltage vector is applied during the first sampling period, and another voltage vector is applied during the second sampling period. In this case, 7^2 sequences of two voltage vectors are possible, as illustrated in Fig. 4(b). This means that a total of 49 possible sequences should be evaluated, which will lead to difficulties in experimental implementation as it requires a large amount of calculations.

To reduce the computational burden, a simplified two-step prediction is employed here. In this scheme, the same voltage vector is evaluated during the second sampling period [23]. Consequently, only seven voltage vectors are evaluated during the two-step prediction, as depicted in Fig. 4(c). This approach presents a similar performance but with much less switching frequency than evaluating 49 voltage vectors.

The cost function for this modified two-step prediction can be expressed as

$$J = [P^* - P(k+1)]^2 + [Q^* - Q(k+1)]^2 + [P^* - P(k+2)]^2 + [Q^* - Q(k+2)]^2 . \quad (23)$$

Similarly to the one-step horizon prediction, the discrete-time model of the system derived in Section III-A is used to predict the active and reactive powers until time $k+2$ (i.e., two consecutive sampling periods) for eight voltage vectors, and the one which minimizes this cost function is applied. This algorithm is repeated for each sampling period. It can be noted that the one-step delay has been compensated for in the cost function. Therefore, this two-step horizon prediction reduces not only the switching frequency but also the power ripple in the actual digital implementation.

IV. Numerical Simulation

The proposed control strategy was tested in simulation using MATLAB/Simulink. The system parameters are listed in Table I. A constant 300-V dc source was used to simulate the PV output. In the test, the proposed MPDPC strategy is investigated, i.e., the simplified two-step horizon prediction with cost function (23) is used.

TABLE I
System Parameters

Filter resistance	R	0.36 Ω
Filter inductance	L	4.7 mH
Grid voltage	V_g	133V
Voltage frequency	f	50 Hz
DC source voltage	V_{dc}	300 V
Sampling period	T_s	50 μs

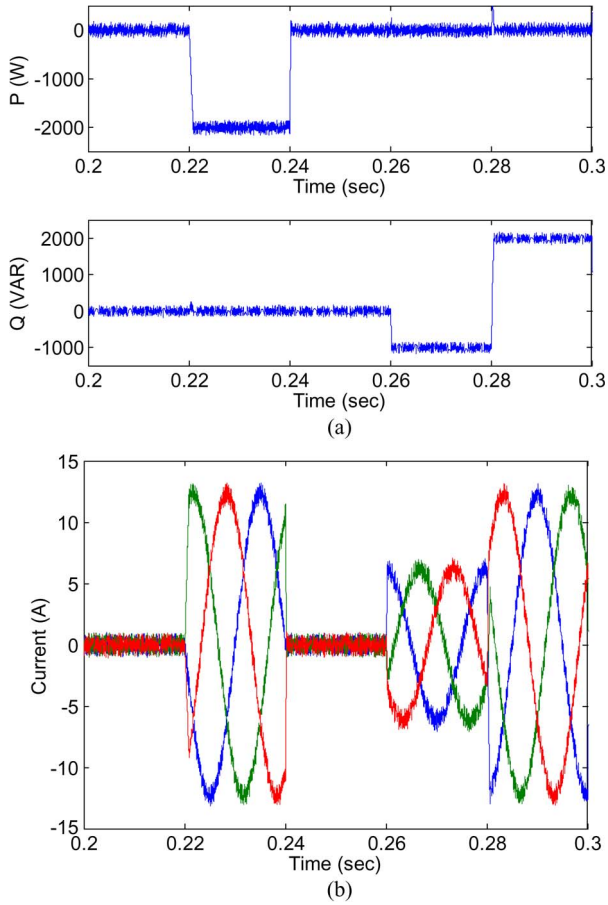

Fig. 5. Simulated dynamic response. (a) Active and reactive powers injected into the grid. (b) Line currents.

Fig. 5 presents the power regulation performance. Initially, the reactive power was set to 0 VAr while the active power was stepped from 0 W to −2 kW at 0.22 s and stepped back to 0 W at 0.24 s. After that, the active power was kept at 0 W while the reactive power was stepped down to −1 kVar and then stepped up to 2 kVAr. It can be seen that the proposed MPDPC strategy produces an excellent dynamic response; the actual powers are very fast at tracking the references with an absolute absence of overshoot currents. Fig. 6 shows the spectrum of the line current in steady state with $P^* = -1$ kW and $Q^* = -1$ kVAr. It can be observed that the current injected into the grid is very sinusoidal with a total harmonic distortion (THD) of only 2.87%.

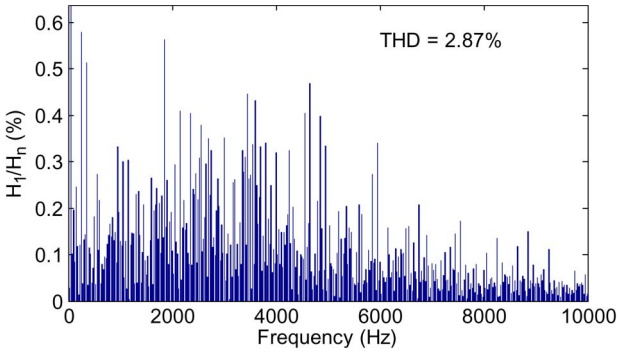

Fig. 6. Line current spectrum in steady state.

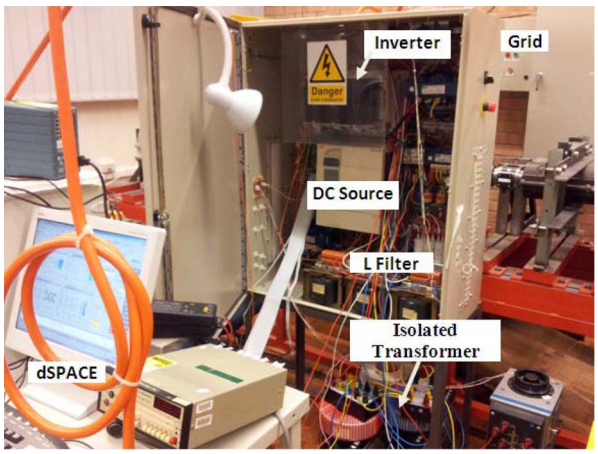

Fig. 7. Laboratory setup.

V. Experimental Verification

The proposed control strategy was further validated by experiment using a laboratory PV system setup, as shown in Fig. 7. It consists of the following devices: a three-phase Semikron intelligent insulated-gate bipolar transistor power module as the inverter, an ABB dc power source, a three-phase L filter, an overcurrent protection device, and a three-phase isolated transformer to increase the inverter output voltage from 133 to 415 V for main grid connection. A dSPACE DS1104 PowerPC/digital signal processor (DSP) control board was employed to implement the real-time algorithm coding using C language for the control. The voltages and currents are sampled using ControlDesk, which is interfaced with the DS1104 and a PC at a sampling rate of $f_s = 20$ kHz. The system parameters are kept the same as the simulation. For easy illustration, the complete block diagram of the controller for experimental implementation is shown in Fig. 8, which is actually the description of Fig. 2(b) in detail. After the voltage vector is selected according to the cost function, the block "Pulses Generation" is used to generate the pulsewidth-modulation (PWM) signals. For instance, when $\boldsymbol{V}_2(110)$ is determined, it can be generated just simply by turning on the upper switch and turning off the bottom switch of leg A of the inverter, and turning on the upper switch and turning off the bottom switch of leg B, and turning off the upper switch and turning on the bottom switch of leg C.

Since conventional SDPC [6] has had a great impact on the technology and is commonly used, it is used here as a benchmark for the proposed MPDPC strategy to compare to. It can be noted that the simplified two-step horizon prediction with cost function (23) was employed for the MPDPC approach in the experimental tests put forward here, unless explicitly indicated otherwise.

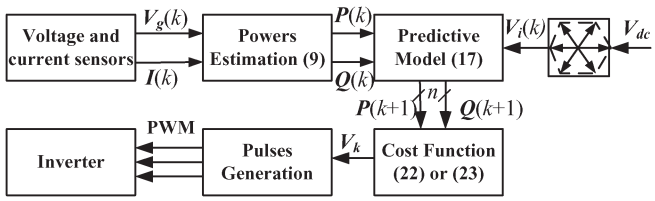

Fig. 8. Complete block diagram of the proposed MPDPC controller.

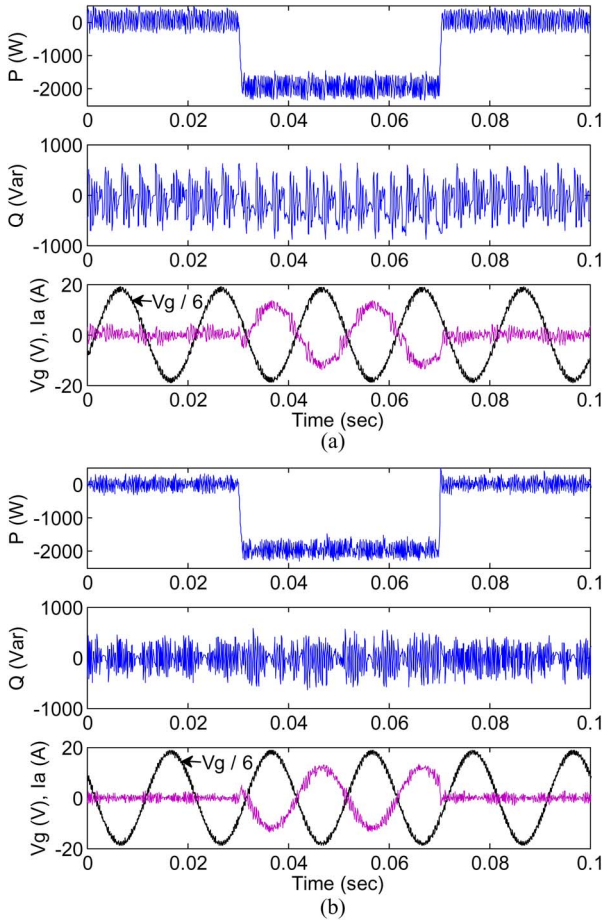

Fig. 9. Experimental dynamic response. (a) SDPC. (b) MPDPC.

A. Flexible Power Regulation

In the experimental tests, a severe active power variation was demanded, and the control strategies driving the grid-connected inverter react in a quick and safe manner. The selected active power variation is a step of 2 kW while the reactive power is kept constant. Fig. 9 shows the transient response of both control strategies. From top to bottom, the curves presented are active power, reactive power, grid voltage, and line current. For the SDPC, the inverter switching states are selected according to a lookup table. The active and reactive powers are controlled directly without coordinate transformation and

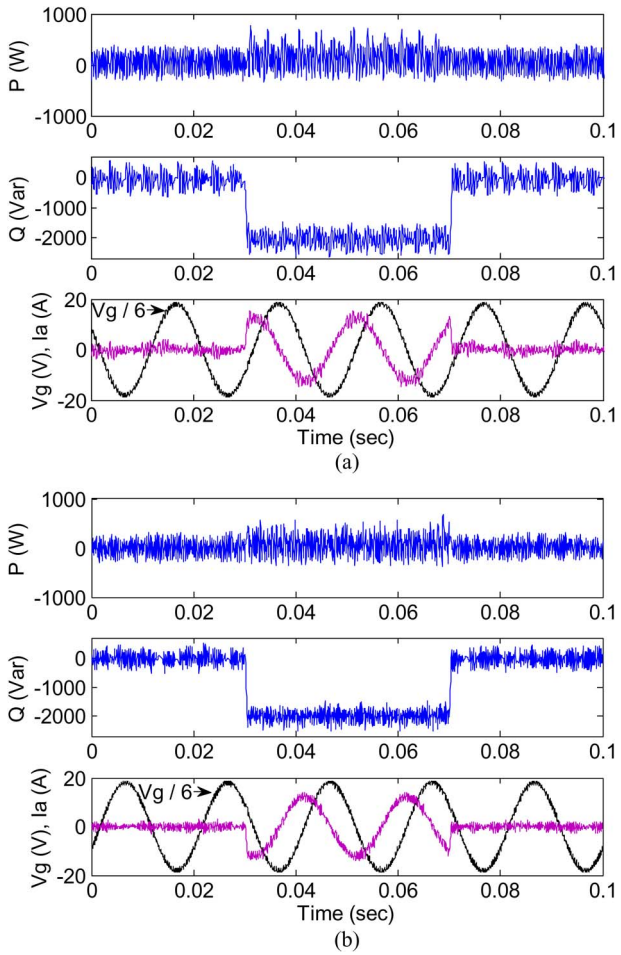

Fig. 10. Experimental dynamic response with changing reactive power commands. (a) SDPC. (b) MPDPC.

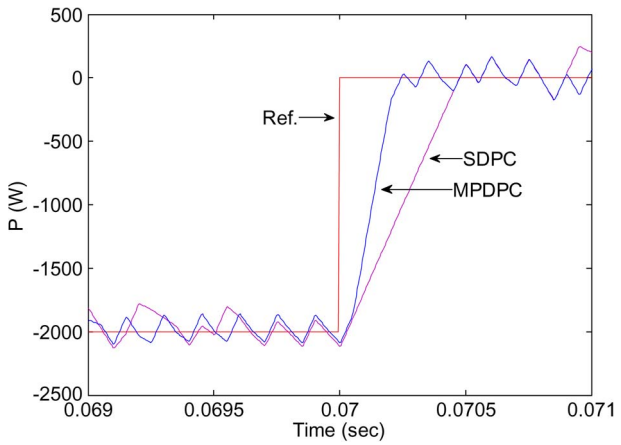

Fig. 11. Zoomed responses of SDPC and proposed MPDPC with step change of active powers.

PWM modulators; hence, a quick dynamic performance can be achieved. From Fig. 9(a) and (b), it can be seen that both SDPC and MPDPC permit a fast and safe transient response, thus demonstrating the excellent dynamic performance of the proposed MPDPC strategy. On the other hand, the results of reactive power commanded are presented in Fig. 10. Similarly, a fast and safe transient response can be achieved.

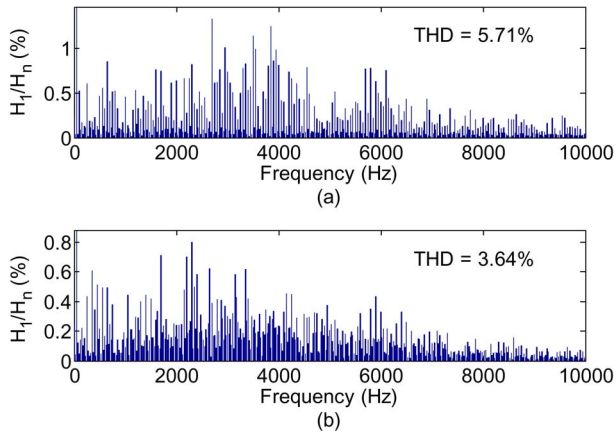

Fig. 12. Comparison of line current spectra in steady state. (a) SDPC. (b) MPDPC.

TABLE II
QUANTITATIVE COMPARISON OF DIFFERENT CONTROL STRATEGIES IN EXPERIMENT

Strategies	f_s (Hz)	f_{sw} (Hz)	THD (%)	P_{rip} (W)	Q_{rip} (Var)
SDPC	20 k	3.32 k	5.71	68.84	92.06
MPDPC.I	20 k	3.41 k	3.10	61.90	60.53
MPDPC.II	20 k	1.72 k	3.64	67.23	61.75

To prove the superiority of the proposed MPDPC compared to SDPC in transient response, the waveforms of the active powers at around 0.07 s are zoomed and plotted in Fig. 11. It can be seen that the proposed MPDPC method has a quicker dynamic response than that of SDPC.

Fig. 12 compares the line current spectra for the SDPC and MPDPC methods in steady state. It is found that both SDPC and MPDPC have broad harmonic spectra. However, the power quality of MPDPC is improved significantly with a THD of only 3.6%.

B. Switching Frequency Reduction

In order to validate the effectiveness of the switching frequency reduction scheme, several tests have been carried out separately. For ease of illustration, the MPDPC strategy using cost function (22) with prediction horizon $N = 1$ is donated as MPDPC.I, while the MPDPC strategy using cost function (23) with prediction horizon $N = 2$ is donated as MPDPC.II. The quantitative comparison is summarized in Table II. This includes the average switching frequency $f_{\rm sw}$, line current THD, active power ripple, and reactive power ripple. The average switching frequency is obtained using the formula $f_{\rm sw} = N/6/0.05/2$, where N is the total switching instants of the six inverter legs during a fixed period of 0.05 s. The power ripples $P_{\rm rip}$ and $Q_{\rm rip}$ are calculated using standard deviation.

From Table II, it is found that the best overall THD improvement is when using MPDPC.I. It has almost the same switching frequency (3.4 kHz) when compared to SDPC. This is as expected because the MPDPC controller selects the most appropriate voltage vector based on a cost function rather than choosing the vector according to a predefined lookup table. If the

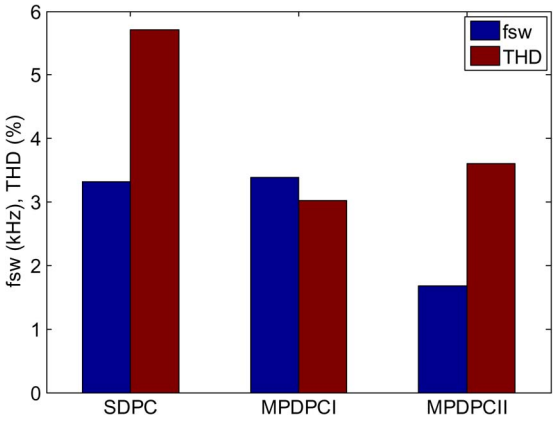

Fig. 13. Comparison of switching frequency and line current.

switching frequency reduction is considered, i.e., MPDPC.II is used, the switching frequency is reduced considerably to only 1.7 kHz with slight deterioration in terms of current THD and power ripple compared to MPDPC.I. To obtain an intuitive view, the switching frequencies and current THDs are further compared in Fig. 13. It can be seen that the power quality of the current injected into the grid is improved, with almost half of the switching frequency compared to SDPC. This shows the effectiveness of the switching frequency reduction scheme.

VI. Conclusion

This paper has proposed an MPDPC method with excellent transient and steady-state performance. Using this method, a grid-connected inverter system can achieve flexible power regulation and switching frequency reduction. The controller is simple and effective. It uses a system model to predict the system behavior; a cost function is then utilized to select the most effective voltage vector. Consequently, no coordinate transformation and proportional–integral regulators are needed, and no switching table and PWM modulators are involved. Both simulation and experimental results are provided to validate the effectiveness of the proposed control strategy, showing that it is very suitable for distributed renewable power generation.

References

[1] F. Blaabjerg, M. Liserre, and K. Ma, "Power electronics converters for wind turbine systems," *IEEE Trans. Ind. Appl.*, vol. 48, no. 2, pp. 708–719, Mar./Apr. 2012.

[2] J. Hu *et al.*, "Predictive direct virtual torque and power control of doubly fed induction generators for fast and smooth grid synchronization and flexible power regulation," *IEEE Trans. Power. Electron.*, vol. 28, no. 7, pp. 3182–3194, Jul. 2013.

[3] S. B. Kjaer, J. K. Pedersen, and F. Blaabjerg, "A review of single-phase grid-connected inverters for photovoltaic modules," *IEEE Trans. Ind. Appl.*, vol. 41, no. 5, pp. 1292–1306, Sep./Oct. 2005.

[4] J. Hu, J. Zhu, and G. Platt, "Smart grid—The next generation electricity grid with power flow optimization and high power quality," in *Proc. IEEE ICEMS*, Aug. 2011, pp. 1–6.

[5] J. Hu, J. Zhu, D. G. Dorrell, and J. M. Guerrero, "Virtual flux droop method—A new control strategy of inverters in microgrids," *IEEE Trans. Power Electron.*, vol. 29, no. 9, pp. 4704–4711, Sep. 2014.

[6] F. Blaabjerg and J. M. Guerrero, "Smart grid and renewable energy systems," in *Proc. IEEE ICEMS*, Aug. 2011, pp. 1–10.

[7] T. Noguchi, H. Tomiki, S. Kondo, and I. Takahashi, "Direct power control of PWM converter without power-source voltage sensors," *IEEE Trans. Ind. Appl.*, vol. 34, no. 3, pp. 473–479, May./Jun. 1998.

[8] M. Malinowski, M. Jasinski, and M. P. Kazmierkowski, "Simple direct power control of three-phase PWM rectifier using space-vector modulation (DPC-SVM)," *IEEE Trans. Ind. Electron.*, vol. 51, no. 2, pp. 447–454, Apr. 2004.

[9] D. Zhi, L. Xu, and B. W. Williams, "Improved direct power control of grid-connected DC/AC converters," *IEEE Trans. Power Electron.*, vol. 24, no. 5, pp. 1280–1292, May 2009.

[10] J. Alonso-Martinez, J. Eloy-Garcia, and S. Arnaltes, "Table-based direct power control: A critical review for microgrid applications," *IEEE Trans. Power Electron.*, vol. 25, no. 12, pp. 2949–2916, Dec. 2010.

[11] P. Cortes, J. Rodriguez, P. Antoniewicz, and M. Kazmierkowski, "Direct power control of an AFE using predictive control," *IEEE Trans. Power Electron.*, vol. 23, no. 5, pp. 2516–2523, Sep. 2008.

[12] J. Hu, J. Zhu, G. Platt, and D. G. Dorrell, "Model-predictive direct power control of AC/DC converters with one step delay compensation," in *Proc. 38th IEEE IECON*, Oct. 2012, pp. 4874–4879.

[13] J. Hu, J. Zhu, G. Lei, G. Platt, and D. G. Dorrell, "Multi-objective model-predictive control for high power converters," *IEEE Trans. Energy Convers.*, vol. 28, no. 3, pp. 652–663, Sep. 2013.

[14] T. Geyer, "A comparison of control and modulation schemes for medium-voltage drives: Emerging predictive control concepts versus PWM-based schemes," *IEEE Trans. Ind. Appl.*, vol. 47, no. 3, pp. 1380–1389, May/Jun. 2011.

[15] Y. Zhang, J. Zhu, and W. Xu, "Predictive torque control of permanent magnet synchronous motor drive with reduced switching frequency," in *Proc. IEEE ICEMS*, Oct. 2010, pp. 798–803.

[16] P. Cortés *et al.*, "Model predictive control of an inverter with output LC filter for UPS applications," *IEEE Trans. Ind. Electron.*, vol. 56, no. 6, pp. 1875–1883, Jun. 2009.

[17] I. S. Mohamed, S. A. Zaid, M. F. Abu-Elyazeed, and H. M. Elsayed, "Model predictive control—A simple and powerful method to control UPS inverter applications with output LC filter," in *Proc. Electron., Commun. Photon. Conf.*, Apr. 2013, pp. 1–6.

[18] J. Rodríguez *et al.*, "Predictive current control of a voltage source inverter," *IEEE Trans. Ind. Electron.*, vol. 54, no. 1, pp. 495–503, Feb. 2007.

[19] M. Preindl, E. Schaltz, and P. Thogersen, "Switching frequency reduction using model predictive direct current control for high-power voltage sources inverters," *IEEE Trans. Ind. Electron.*, vol. 58, no. 7, pp. 2826–2835, Jul. 2011.

[20] J. Scoltock, T. Geyer, and U. Madawala, "Model predictive direct power control for a grid-connected converter with an LCL-filter," in *Proc. IEEE ICIT*, Feb. 2013, pp. 588–593.

[21] N. Mohan, T. M. Undeland, and W. P. Robbins, *Power Electronics*. Hoboken, NY, USA: Wiley, 2003.

[22] W. Kramer, S. Chakraborty, B. Kroposki, and H. Thomas, "Advanced power electronic interfaces for distributed energy systems—Part 1: Systems and topologies," Nat. Renewable Energy Lab., Golden, CO, USA, Rep. NREL/TP-581-42672, Mar. 2008.

[23] P. Cortes, J. Rodriguez, S. Vazquez, and L. G. Franquelo, "Predictive control of a three-phase UPS inverter using two steps prediction horizon," in *Proc. IEEE Int. Conf. Ind. Technol.*, Mar. 2010, pp. 1283–1288.

Jiefeng Hu (S'12–M'14) received the Ph.D. degree in electrical engineering from the University of Technology Sydney (UTS), Sydney, Australia, in 2013.

From January 2011 to March 2013, he was involved in the research of minigrids in the Commonwealth Scientific and Industrial Research Organisation, Clayton, Vic., Australia. From July 2013 to June 2014, he was a Research Associate with UTS. Since March 2014, he has been with Beijing University of Aeronautics and Astronautics (Beihang University), Beijing, China, as an Associate Professor. His research interests include electric drives, control of power converters, and smart microgrids.

Dr. Hu was conferred the N.S.W./A.C.T. Postgraduate Student Energy Awards by the Australian Institute of Energy in October 2010.

Jianguo Zhu (S'93–M'96–SM'03) received the B.E. degree in electrical engineering from Jiangsu Institute of Technology, Jiangsu, China, in 1982, the M.E. degree in electrical engineering from Shanghai University of Technology, Shanghai, China, in 1987, and the Ph.D. degree in electrical engineering from the University of Technology Sydney (UTS), Sydney, N.S.W., Australia, in 1995.

He is currently a Professor of electrical engineering and the Head of the School of Electrical, Mechanical and Mechatronic Systems, UTS. His research interests include electromagnetics, magnetic properties of materials, electrical machines and drives, power electronics, and green energy systems.

David G. Dorrell (M'95–SM'08) received the Ph.D. degree in engineering from the University of Cambridge, Cambridge, U.K., in 1993.

He is currently an Associate Professor with the University of Technology Sydney, N.S.W., Sydney, Australia. His research interests cover the design and analysis of various electrical machines and also renewable energy systems.

Dr. Dorrell is a Chartered Engineer in the U.K. and a Fellow of the Institution of Engineering and Technology, U.K.